Journal of Bioscience and Bioengineering
VOL. 128 No. 4, 410–415, 2019

ELSEVIER

www.elsevier.com/locate/jbiosc

Oligomerization of a modular ribozyme assembly of which is controlled by a programmable RNA–RNA interface between two structural modules

Ryusei Tsuruga,[1] Narumi Uehara,[2] Yuki Suzuki,[3] Hiroyuki Furuta,[2] Hiroshi Sugiyama,[3,4] Masayuki Endo,[4] Shigeyoshi Matsumura,[1] and Yoshiya Ikawa[1,*]

Department of Chemistry, Graduate School of Science and Engineering, University of Toyama, 3190 Gofuku, Toyama 930-8555, Japan,[1] Department of Chemistry and Biochemistry, Graduate School of Engineering, Kyushu University, 744 Moto-oka, Nishi-ku, Fukuoka 819-0395, Japan,[2] Department of Chemistry, Graduate School of Science, Kyoto University, Kyoto 606-8502, Japan,[3] and Institute for Integrated Cell-Material Sciences (iCeMS), Kyoto University, Kyoto 606-8502, Japan[4]

Received 2 March 2019; accepted 2 April 2019
Available online 17 May 2019

Bimolecular ribozymes derived by physical dissection of unimolecular ribozymes consisting of two structural modules are promising platforms for the design and construction of assembled RNA nanostructures. Unit RNAs to be assembled intermolecularly into one-dimensional (1D) oligomers are designed by reconnecting the two structural modules in a manner different from the parent ribozymes. This strategy was applied to the *Tetrahymena* group I ribozyme. We constructed 1D ribozyme oligomers the assembly of which was observed by atomic force microscopy (AFM) and also controlled rationally to design a heterooctamer by differentiating the interface between the two modules.

[**Keywords:** Catalytic RNA; Group I intron; Ribozyme; RNA nanostructure; RNA nanotechnology]

Structured RNA molecules identified from living organisms are promising platforms for the design and construction of nanosized structures and their assemblies (1–5), some of which could be applicable in nanobiotechnology and nanomedicine (6–10). Among naturally occurring RNA structures, group I self-splicing intron RNAs belong to a category of large RNA enzymes (ribozymes) (11). They are usually over 200 nucleotides in length and have important biological roles. Group I intron ribozymes have a modular architecture, in which multiple short helical elements assemble to build complex three-dimensional (3D) structures (12–15). Their modular 3D structures can be dissected into two or more structural modules, each of which undergoes self-folding without the assistance of its partner module(s) and ribozyme functions can be reconstituted by assembly of the modular RNAs through noncovalent tertiary interactions (16–20).

Rational engineering of a group I intron from *Tetrahymena thermophila* (*Tetrahymena* group I ribozyme) has been examined to design assembled RNA nanostructures with catalytic functions (21,22). A bimolecular version of the *Tetrahymena* ribozyme (P5abc/ΔP5 bimolecular ribozyme) consisting of two modular RNAs has been used to design ribozyme oligomers (16,17). Artificial reconnection of two modular RNAs allows them to coexist in one molecule but prohibits their intramolecular assembly (Fig. 1A). The two modules in an engineered ribozyme are thus allowed to assemble only in an intermolecular manner. Using this design strategy, the *Tetrahymena* group I ribozyme has been engineered to undergo homooligomerization to form a closed trimer and closed tetramer (21,22). The resulting engineered ribozyme exhibited its catalytic ability depending on the formation of its oligomeric states with triangle and square shapes. This observation seems similar to biochemical properties of protein oligomers (23). In the case of hemoglobins serving as oxygen transporter, the extent of their oligomerization is significantly diversified during their evolution and it ranges from single subunit to 180-subunit to adapt their oxygen-binding properties and protein stabilities to given environments (24).

Oligomerization of hemoglobin proteins is conceptually applicable to RNA-based enzymes as a strategy to modulate their functions and stabilities, which may be tuned finely depending on the extent of oligomerization. As the initial step to exploit this strategy, it is important to design and construct oligomeric forms of modular ribozymes and also to control the extent of their oligomerization. In this study, we first designed and analyzed one-dimensional (1D) assembly of an engineered ribozyme derived from the P5abc/ΔP5 bimolecular ribozyme as the simplest form of ribozyme oligomers. As a simple but affective strategy to control the extent of protein oligomerization, distinct module–module interfaces were developed to generate heterooligomers from homooligomers (25). In this study, we rationally increased the number of distinct RNA–RNA interfaces between two structural modules of the P5abc/ΔP5 ribozyme. They enable us to design RNA nanostructures with different extents of oligomerization through controlled assembly of their structural modules.

MATERIALS AND METHODS

Molecular design The crystal structure of the *Tetrahymena* group I ribozyme (PDB ID: 1X8W) was used for construction of three-dimensional models of H1 RNA

* Corresponding author. Tel.: +81 76 445 6599; fax: +81 76 445 6549.
E-mail address: yikawa@sci.u-toyama.ac.jp (Y. Ikawa).

1389-1723/$ – see front matter
https://doi.org/10.1016/j.jbiosc.2019.04.003

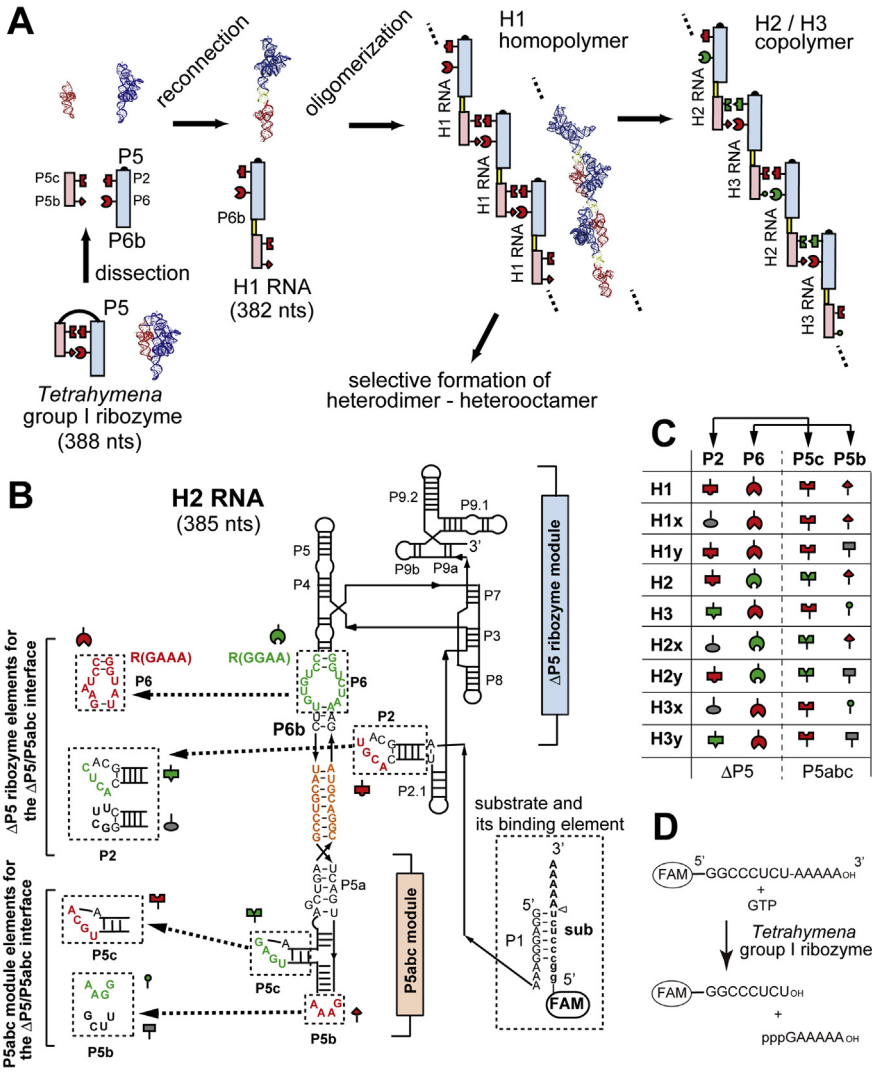

FIG. 1. Design of 1D oligomers based on engineered ribozymes derived from the *Tetrahymena* group I ribozyme. (A) Scheme of modular redesign to generate engineered group I ribozymes that can show 1D oligomerization. In the scheme, nts stands for nucleotides. (B) Secondary structure of an engineered group I ribozyme (H2 RNA). Arrowheads superimposed on solid lines indicate 5′-to-3′ polarity. Boxes with broken lines indicate modularly replaceable RNA elements to derive variants from the parent H1 RNA. Broken lines with arrowheads indicate RNA elements used to design derivatives of H1 RNA. Nucleotides shown in orange indicate linker duplexes. Nucleotides shown in red represent the RNA motifs that are present in the wild-type *Tetrahymena* group I ribozyme and also in H1 RNA. Nucleotides shown in green and thick black indicate RNA elements that were artificially introduced for modular engineering. (C) RNA–RNA tertiary interactions that constitute RNA–RNA interfaces between the ΔP5 ribozyme module and the P5abc module. Elements shown in red are the RNA motifs present in the wild-type *Tetrahymena* group I ribozyme and in H1 RNA. Elements shown in green are the motifs artificially introduced for modular engineering to produce H2 and H3 RNAs. UUCG tetraloops used to disrupt the tertiary interactions are shown in gray. (D) The substrate cleavage reaction catalyzed by the *Tetrahymena* group I ribozyme. FAM fluorophore was linked covalently to the 5′-end of the substrate RNA to visualize its cleavage.

and its oligomeric state. Discovery Studio (Accelrys Software Inc., San Diego, CA, USA) was used to perform molecular modeling.

Plasmid construction and RNA preparation Plasmids encoding sequences of H1 RNA and its derivatives were derived from pTZIVSU encoding the *Tetrahymena* group I intron (26). Each plasmid was generated by PCR-based mutagenesis. These plasmids were then used as PCR templates to prepare DNA fragments for transcription with T7 RNA polymerase. The sense PCR primer contained the T7 promoter sequence. PCR-amplified DNA templates were used for synthesis of H1 RNA and its derivatives by *in vitro* transcription. The transcribed RNA was purified on a 4% denaturing polyacrylamide gel. 3′-end labeling of RNAs with BODIPY-fluorophore was performed according to the published protocol (27).

Gel electrophoresis mobility shift assay Electrophoretic mobility shift assays (EMSAs) were performed to analyze assembly of H1-RNA and its derivatives according to the procedure reported by Oi et al. (21). Electrophoresis was performed at 4 °C, 200 V for the initial 5 min, followed by 75 V for 5 h except in the experiment shown in Fig. 4B where electrophoresis was performed for 12 h. The binding affinity of the P5abc module and the ΔP5 module were varied considerably depending on the identity of the P5abc/ΔP5 interface (22,28). Stability of the interface can be improved by increasing Mg^{2+} concentration (22,28), which also enhances mismatched interactions (22,28). In each EMSA, we therefore tuned the concentration of Mg^{2+}, under which the weakest P5abc/ΔP5 interface in a given oligomer was formed stably but stronger P5abc/ΔP5 interfaces did not form mismatched interactions.

Ribozyme activity assay An appropriate set of aqueous RNA solutions, each of which (final concentration: 0.5 μM) was heated separately at 80 °C for 5 min, was mixed at 37 °C. The 10× concentrated reaction buffer (final concentrations: 30 mM Tris–HCl, pH 7.5, and 3.75 mM $MgCl_2$) and 2 mM guanosine triphosphate (final concentration: 0.2 mM) were added to the RNA solution and incubated at 37 °C for 30 min. Ribozyme reactions were initiated by adding the RNA substrate (5′-GGCCCUCUAAAAA-3′), the 5′-end of which was labeled with FAM (carboxyfluorescein, final concentration: 0.5 μM) and allowed to react at 37 °C. Aliquots were taken at given time points and the mixtures were electrophoresed on 15% denaturing polyacrylamide gels. The mean values are indicated in the figures with the minimal and maximal values are shown by error bars. The activity of the ribozyme unit was conducted partially by unstable and transient association between the P5abc module and the ΔP5 module (29). The partial activity of the ΔP5 ribozyme unit was also conducted in the presence of 5 mM Mg^{2+}, under which unstable and transient formation of the active structure of the ΔP5 ribozyme was induced (30). We therefore employed 3.75 mM Mg^{2+} for the activity assay although it was distinctly lower than Mg^{2+} concentrations for stable formation

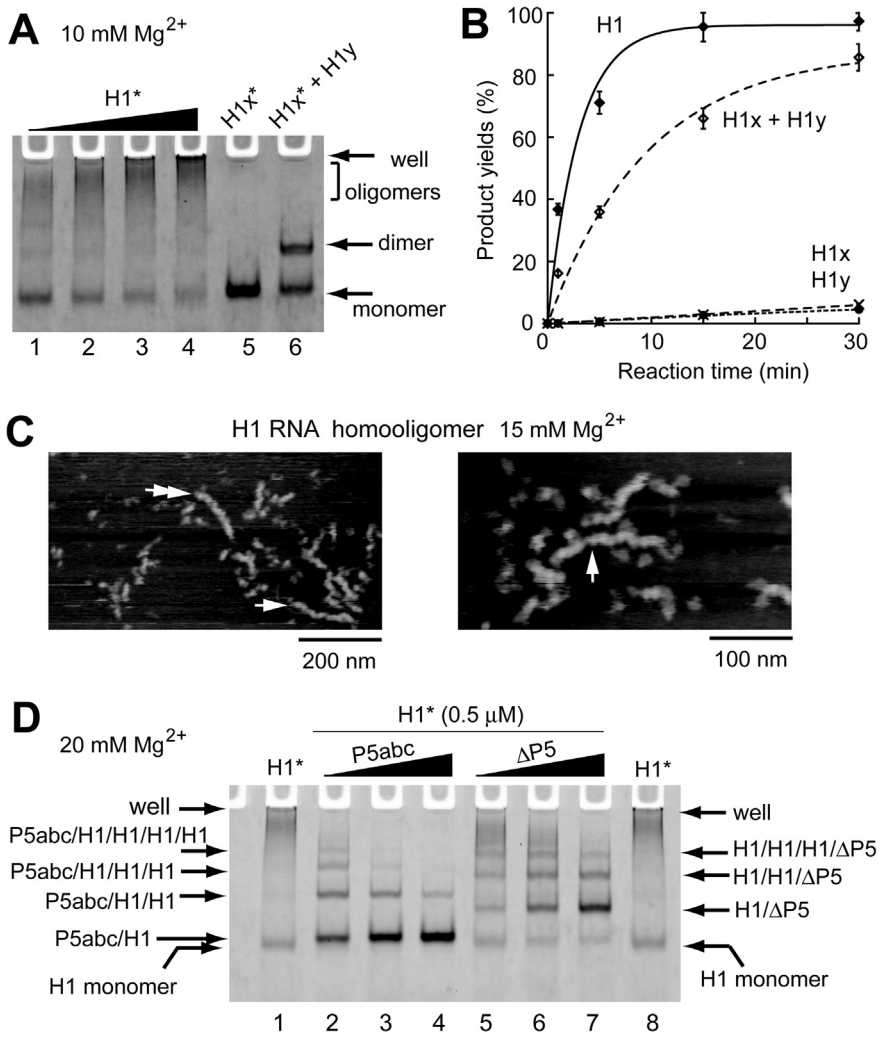

FIG. 2. Formation of 1D oligomers by homooligomerization of H1 RNA. (A) EMSA of H1 RNA and its mutants. EMSA in the presence of 10 mM Mg^{2+}. Asterisks indicate monomer RNAs labeled with BODIPY fluorophore. In lanes 1, 2, 3, and 4, the concentrations of H1 RNA are 0.25, 0.5, 1.0, and 2.0 μM, respectively. In lane 5, the concentration of H1x RNA is 0.5 μM. In lane 6, concentrations of H1x RNA + H1y RNA are 0.25 + 0.25 μM. (B) Reactions to cleave the substrate RNA by H1 RNA and its mutants (H1x and H1y). In reactions catalyzed by H1, H1x, or H1y, the concentration of ribozyme RNA was 0.5 μM. In the reaction with H1x + H1y, the concentrations of H1x and H1y were both 0.25 μM. (C) AFM of H1 RNA homooligomerization in the presence of 15 mM Mg^{2+}. (D) Disassembly of H1 homooligomers by P5abc RNA and ΔP5 RNA acting as competitive stoppers. In lanes 2–4, concentrations of P5abc RNA are 0.25, 0.5, and 1.0 μM, respectively. In lanes 5–7, concentrations of ΔP5 RNA are 0.25, 0.5, and 1.0 μM, respectively. In lanes 1 and 8, the concentration of H1 RNA is 0.5 μM.

of P5abc/ΔP5 interfaces for H1 homooligomer (10 mM) and H2 + H3 copolymer (20 mM) in EMSA.

Atomic force microscopy Atomic force microscopy (AFM) was performed on a high-speed AFM (Nano Live Vision; RIBM, Tsukuba, Japan) according to the protocol reported by Oi et al. (21). The RNA samples were diluted to a final concentration of ~80 nM in folding buffer containing 15 mM Mg^{2+}, and 2 μL of the sample was deposited onto the mica surface of the AFM (21).

RESULTS AND DISCUSSION

Design of H1 RNA homooligomerization We redesigned the P5abc/ΔP5 ribozyme to construct a 1D array of the modular ribozyme consisting of two structural modules (P5abc and ΔP5) (16,17). To apply the P5abc/ΔP5 assembly as an interface to support intermolecular RNA assembly, we reconnected the P5a element in the P5abc module to the P6b element in the ΔP5 module through a rigid duplex linker (Fig. 1A and B). In the resulting variant (H1 RNA) and a series of its derivatives (H-RNA series, Fig. 1C), the P5abc and ΔP5 modules could assemble only in an intermolecular manner, resulting in the formation of a 1D assembly of H1 RNA. The resulting 1D array of H1 RNA exhibited catalytic activity comparable to that of the P5abc/ΔP5 bimolecular ribozyme because the P5abc/ΔP5 bimolecular ribozyme has a repeated structure in the assembled H1 RNA (Fig. 1A).

We first performed EMSA of H1 RNA in the presence of Mg^{2+} to examine its homooligomer formation (Fig. 2A). In the presence of 10 mM Mg^{2+}, H1 RNA showed a monomer band under conditions of low RNA concentration (Fig. 2A, lane 1). The amount of monomer decreased gradually with increases in H1 RNA concentration (Fig. 2A, lanes 2–4). A broad band with low mobility was also observed, the mobility of which decreased gradually in a concentration-dependent manner (Fig. 2A). These observations suggested the formation of H1 RNA homooligomer in an H1 RNA concentration-dependent manner. Further increases in H1 RNA concentration formed an additional band that remained in the well (Fig. 2A, lanes 3 and 4), suggesting the formation of longer oligomers that were too large to migrate into the polyacrylamide gel matrix. Homooligomerization of H1 RNA appeared to be enhanced in the presence of Mg^{2+} at concentrations higher than 10 mM (Fig. S1A and B). This observation was also consistent with the

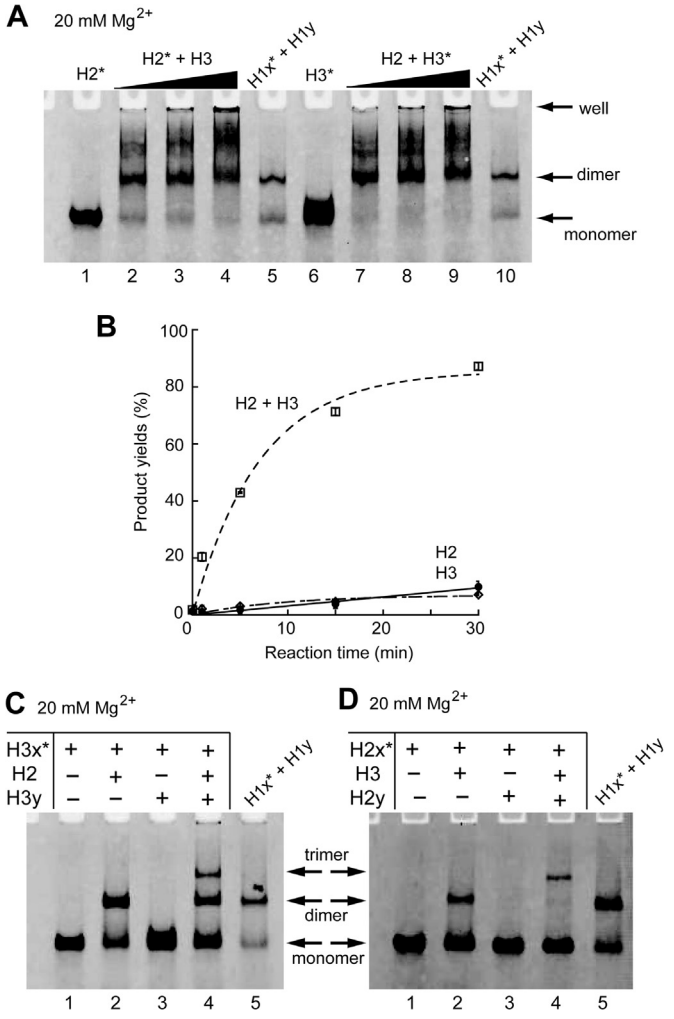

FIG. 3. Formation of 1D copolymers by H2 RNA and H3 RNA. (A) EMSA of H2 RNA + H3 RNA was performed in the presence of 20 mM Mg^{2+}. Asterisks indicate monomer RNAs labeled with BODIPY fluorophore. In lanes 1, 5, 6, and 10, concentrations of H2, H3, H1x, and H1y are 0.25 μM. Concentrations of H2 RNA + H3 RNA are 0.25 + 0.25 μM in lanes 2 and 7, 0.5 + 0.5 μM in lanes 3 and 8, and 1.0 + 1.0 μM in lanes 4 and 9, respectively. (B) Reactions to cleave the substrate RNA by H2 RNA and H3 RNA. In reactions catalyzed by H2 or H3, the ribozyme RNA concentration was 0.5 μM. In the reaction with H2 + H3, the concentrations of H2 and H3 were both 0.5 μM. (C) Selective formation of an H-RNA trimer consisting of H3x, H2, and H3y RNA. Concentrations of H3x, H2, H3y, H1x, and H1y are 0.25 μM. (D) Selective formation of an H-RNA trimer consisting of H2x, H3, and H2y RNA. Concentrations of H2x, H3, H2y, H1x, and H1y are 0.25 μM.

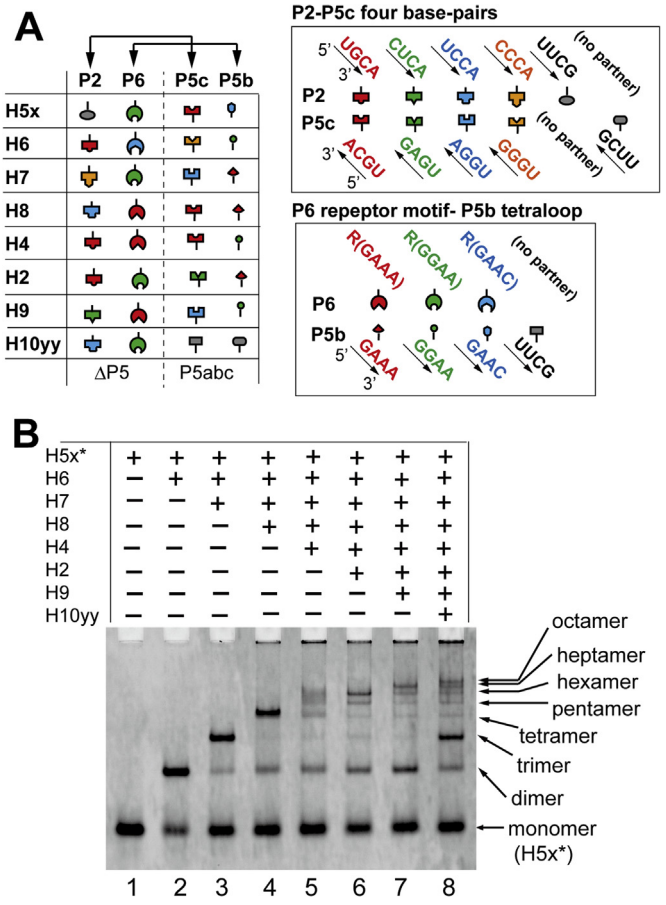

FIG. 4. Selective formation of H-RNA heterooctamer through the assembly of eight distinct H-RNAs. (A) RNA–RNA tertiary interactions that constitute RNA–RNA interfaces between the ΔP5 ribozyme module and the P5abc module. (B) EMSA of eight distinct H-RNAs performed in the presence of 50 mM Mg^{2+}. The order of listed monomers and their presence indicated by plus (+) are consistent with their order in the heterooctamer and oligomers (monomer to heptamer) that were formed as parts of the heterooctamer. For instance, the major tetramer band in lane 4 corresponds to the H5x/H6/H7/H8 heterotetramer. Asterisk indicates that H5 RNA is labeled with BODIPY fluorophore. The concentration of each H-RNA is 0.25 μM.

general property of RNA folding and assembly in that the stability of RNA tertiary interactions is dependent on Mg^{2+} concentration (28).

To evaluate the oligomerization of H1 RNA, we designed a control molecule incapable of homooligomer formation. H1x RNA, in which the P2 element was substituted with a UUCG loop (Fig. 1C) (31), was designed to disrupt the P5abc/ΔP5 interfaces in the H1 homooligomer. Although H1x RNA alone formed no oligomers (Fig. 2A, lane 5), H1x RNA was expected to form a heterodimer with H1y RNA bearing a disrupted P5b element (Figs. 1C and S2C). H1y RNA, the homolytic assembly of which is also unstable due to a defective P5abc/ΔP5 interface lacking P6/P5b interaction, can form the intact P5abc/ΔP5 interface with H1x RNA using the P5abc module in H1x RNA and the ΔP5 module in H1y RNA (Fig. 1C). Addition of unlabeled H1y RNA to fluorescently labeled H1x RNA yielded a new band corresponding to the H1x/H1y heterodimer without the formation of higher oligomer bands (Fig. 2A, lane 6).

We next evaluated the oligomerization ability of H1 RNA and its two mutants by monitoring the catalytic activity of the P5abc/ΔP5 ribozyme unit formed in the oligomers (Fig. 2B). In the presence of 3.75 mM Mg^{2+}, H1x RNA (0.5 μM) or H1y RNA (0.5 μM) hardly promoted the substrate cleavage reaction (Fig. 2B), in which GTP served as a nucleophile to cleave the substrate RNA (0.5 μM) (Fig. 1D) (32). In the presence of equimolar amounts of H1x RNA (0.25 μM) and H1y RNA (0.25 μM), however, cleavage of the substrate RNA (0.5 μM) proceeded smoothly (Fig. 2B). This activity originated from formation of the active ribozyme unit through assembly of the P5abc module in H1x RNA and the ΔP5 module in H1y RNA. Under the same reaction conditions, H1 RNA also exhibited catalytic activity (Fig. 2B), which was twofold higher than that of the H1x/H1y heterodimer. This was consistent with the number of active catalytic units formed in the oligomeric states. In the H1 RNA homooligomer, each H1 RNA molecule provided one active catalytic site, which was established by assembly between the ΔP5 module of H1 RNA and the P5abc module of the neighboring H1 RNA (Fig. S2C). In the H1x/H1y heterodimer, however, two RNA molecules provided only one catalytic unit formed by the P5abc module in H1x RNA and the ΔP5 module in H1y RNA (Fig. S2C).

To obtain further evidence regarding the formation of H1 RNA homooligomers, we examined the molecular structure of H1 RNA directly by AFM. In the presence of 15 mM Mg^{2+}, H1 RNA (83 nM) showed 1D array structures of estimated lengths ~150 nm (single

arrowhead in Fig. 2C, left panel), ~135 nm (double arrowhead in Fig. 2C, left panel), and ~130 nm (single arrowhead in Fig. 2C, right panel). In 3D structures of the parent *Tetrahymena* ribozyme and H1 RNA (Fig. S1C), the height of H1 RNA was estimated to be 17.6 nm (Fig. S1C, middle image) and the extension per one H1 RNA molecule was 9.8 nm (Fig. S1C, right image). This strongly suggested that more than 10 H1 RNA molecules were likely to be assembled in the observed AFM images (Fig. 2C). We also observed H2 RNA, in which P6 receptor motif and P5c loop of H1 RNA were mutated to disrupt homooligomerization capability (Fig. 1B). In the presence of 15 mM Mg^{2+}, AFM images of H2 RNA (83 nM) predominantly showed dispersed molecules that corresponded to its monomeric state (Fig. S1D).

To further determine whether the retarded bands in EMSA of H1 RNA were homooligomers, we disassembled the oligomeric states by adding P5abc RNA or ΔP5 RNA (Fig. S2A–C). Both RNAs are structural modules that form a complex with H1 RNA and thus would serve as stopper molecules to prevent H1 RNA homooligomerization in a competitive manner (Fig. S2C). In the oligomeric state of H1 RNA (0.5 μM) with 20 mM Mg^{2+}, we added P5abc RNA or ΔP5 RNA as a stopper molecule, and several distinct bands were newly observed in a stopper RNA dose-dependent manner (Fig. 2D, lanes 2–7). In the presence of 1.0 μM P5abc RNA (Fig. 2D, lane 4) and 1.0 μM ΔP5 RNA (Fig. 2D, lane 7), the dominant band corresponded to the bimolecular complex of P5abc/H1 and H1/ΔP5 (Fig. S2C), respectively. This experiment also enabled us to identify distinct oligomers consisting of two to five RNA molecules (Fig. 2D), indicating that EMSA can be used for the separation of dimers to pentamers in this 1D RNA assembly system.

Design of H2 RNA and H3 RNA and their copolymerization Based on the characterization of H1 homooligomers, we then engineered H1 RNA homopolymer to copolymer consisting of two RNA components (Fig. 1A). For this purpose, we engineered the P5abc/ΔP5 interface to generate a pair of orthogonal interfaces (21,28). We constructed two H1 RNA variants (H2 RNA and H3 RNA) by introducing the second P5b-P6 pair and the second P5c-P2 pair, which are shown in green in Fig. 1 where the original (first) P5b-P6 pair and P5c-P2 pair are shown in red. H2 RNA and H3 RNA were designed as unit RNAs for alternative copolymer formation (Fig. 1). In the H2 RNA and H3 RNA pair, the P5abc module and ΔP5 module of one RNA were designed to interact with ΔP5 and P5abc in the respective partner RNA (Fig. 1C) to lead to the formation of a copolymeric state (Fig. 1A).

Without the partner RNA, H2 RNA (Fig. 3A, lane 1) or H3 RNA (Fig. 3A, lane 6) alone migrated as the monomeric state. In the presence of equimolar amounts of H2 RNA and H3 RNA, retardation of bands were observed (Fig. 3A) and one of these bands corresponded to the dimeric state because its mobility was similar to that of H1x/H1y dimer (Fig. 3A, lanes 5 and 10). These observations indicated the formation of H2/H3 heterooligomer in an H2 RNA and H3 RNA dose-dependent manner (Fig. 3A and S4C). Assembly of H2 RNA and H3 RNA was also confirmed from the catalytic activity in the presence of the two RNAs because H2 RNA or H3 RNA alone showed poor activity (Fig. 3B).

We then examined rational control of the extent of 1D oligomerization beyond the H1x/H1y heterodimer (Fig. 2A, lane 6). By employing two types of mutant H3 RNA, we selectively formed a trimeric state consisting of H3x/H2/H3y (Figs. 3C and S2D), in which H3 mutants (H3x and H3y, Fig. 1C) in both sides in the trimer prevented further oligomerization (Fig. S2D). A trimer bearing H3 RNA in its central position (H2x/H3/H2y, Figs. 3D and S2D) was also prepared in a similar manner using two mutant H2 RNAs (H2x and H2y, Fig. 1C). We additionally examined the selective formation of the trimer using the strongest interface supporting homooligomerization of H1 RNA (Fig. S2D and E). The resulting trio of three RNAs (H1x, H4, and H2y) also formed a trimer (H1x/H4/H2y, Fig. S2E, lane 4). By employing the three of four possible P5abc/ΔP5 interfaces, we further designed the heterotetramer (H1x/H4/H2/H3y, Fig. S2D). Formation of the RNA tetramer was also confirmed in the presence of 20 mM Mg^{2+} (Fig. S2F, lane 4) although its efficiency was limited to 5%.

Expansion of the P5abc/ΔP5 interfaces to selective formation of up to the octamer We then expanded the variety of P5abc/ΔP5 interfaces by introducing the third P2-P5c pair (shown in blue in Fig. S2G), the stability of which was lower than that of the red P2-P5c pair but higher than that of the green P2-P5c pair (22). Among the six possible P5abc/ΔP5 interfaces, we employed five distinct interfaces for the selective formation of a heterohexamer (Figs. S2H and S3A), which could be detected by EMSA in the presence of 20 mM (Fig. S3B and C) or 30 mM Mg^{2+} (Fig. S3D–G). We further extended this type of 1D RNA array to form a heterooctamer by generating seven distinct P5abc/ΔP5 interfaces (Figs. 2H and 4A), which was achieved by introducing the fourth P2-P5b pair (orange P2-P5c pair in Figs. 4A and S2G) and the third P6-P5b pair (GAAC loop and its receptor pair shown in blue in Figs. 4A and S2G) (33).

To minimize uncontrolled extension exceeding the octamer by mismatched interactions, we introduced two UUCG loops into one of the terminal units (H10yy, Fig. 4A). The opposite terminal unit was designed by introducing a UUCG loop into the P2 element (H5x, Fig. 4A). As the formation of longer RNA oligomers was entropically less favored, we increased Mg^{2+} concentration to 50 mM to stabilize the P5abc/ΔP5 interfaces (Fig. 4B, see also Fig. S4A in which an enlarged image of lanes 6–8 in Fig. 4B is shown). H5x RNA was 3′-end labeled with BODIPY fluorophore (27) and used as the terminal component, to which the neighboring components were assembled in designed order (Fig. 4B). Stepwise addition of the RNA component selectively afforded the dimer (Fig. 4B, lane 2), trimer (Fig. 4B, lane 3), tetramer (Fig. 4B, lane 4), hexamer (lane 6 in Figs. 4B and S4A), and heptamer (lane 7). On the other hand, the formation of the pentamer was somewhat unclear (Fig. 4B, lane 5) probably because the ΔP5 module in H4 RNA cause mismatched interactions in the absence of its cognate partner (H2 RNA) and formed hexamer and higher oligomers. In the presence of eight H-RNA components, a weak but detectable band was observed, which corresponded to the heterooctamer (lane 8 in Figs. 4B and S4A). Stepwise formation of the ribozyme octamer also suggested a possible relationship between the number of RNA units in an H-RNA oligomer and the extent of its mobility in the native gel, where there seemed an asymptotic value of the mobility reached by infinite oligomerization (Fig. S4B). This hypothetical relationship, however, reached an impasse because we found that higher H1 RNA homooligomers and higher H2 + H3 copolymers were unable to enter the gel (Fig. S4C). Although the overall yield of the ribozyme octamer was low (Fig. 4B), the seven distinct RNA–RNA interfaces developed in this study (Fig. S2H) would expand the scope of ribozyme-based 2D and 3D nanostructure construction, especially for those with closed-shapes involving a cyclic heptamer and a triangular prism (34–37). To achieve these nanostructures, other modular parts than P5abc/ΔP5 interfaces must be developed to fulfill their geometric requirements.

The current goal of the construction and analysis of the ribozyme 1D-oligomers is to elucidate the relationship between their assembly property and catalytic ability. On the other hand, pharmaceutical application of ribozymes including the *Tetrahymena* group I ribozyme have been investigated (38) although a limited number of researches have been reported on bioavailability of monomeric ribozymes (39). Oligomerization of ribozymes may also modulate the bioavailability of their ribozyme units because an

assembled RNA nanostructure consisting of eight RNA components has been shown to be more resistant to ribonuclease degradation than its component RNAs (3). Integration of the engineered oligomerization and pharmaceutical application must be an attractive but long-term goal of applied studies the *Tetrahymena* group I ribozyme.

Supplementary data to this article can be found online at https://doi.org/10.1016/j.jbiosc.2019.04.003.

ACKNOWLEDGMENTS

This work was supported by MEXT KAKENHI Grant Number JP15K05561 (Y.I.). This work was also supported partly by University of Toyama Discretionary Funds of the President "Toyama RNA Research Alliance" (to Y.I. and S.M.).

References

1. **Hoeprich, S. and Guo, P.:** Computer modeling of three-dimensional structure of DNA-packaging RNA (pRNA) monomer, dimer, and hexamer of Phi29 DNA packaging motor, J. Biol. Chem., **277**, 20794–20803 (2002).
2. **Chworos, A., Severcan, I., Koyfman, A. Y., Weinkam, P., Oroudjev, E., Hansma, H. G., and Jaeger, L.:** Building programmable jigsaw puzzles with RNA, Science, **306**, 2068–2072 (2004).
3. **Severcan, I., Geary, C., Chworos, A., Voss, N., Jacovetty, E., and Jaeger, L.:** A polyhedron made of tRNAs, Nat. Chem., **2**, 772–779 (2010).
4. **Dibrov, S. M., McLean, J., Parsons, J., and Hermann, T.:** Self-assembling RNA square, Proc. Natl. Acad. Sci. USA, **108**, 6405–6408 (2011).
5. **Ishikawa, J., Furuta, H., and Ikawa, Y.:** RNA tectonics (tectoRNA) for RNA nanostructure design and its application in synthetic biology, Wiley Interdiscip. Rev. RNA, **6**, 651–664 (2013).
6. **Afonin, K. A., Kireeva, M., Grabow, W. W., Kashlev, M., Jaeger, L., and Shapiro, B. A.:** Co-transcriptional assembly of chemically modified RNA nanoparticles functionalized with siRNAs, Nano Lett., **12**, 5192–5195 (2012).
7. **Afonin, K. A., Viard, M., Koyfman, A. Y., Martins, A. N., Kasprzak, W. K., Panigaj, M., Desai, R., Santhanam, A., Grabow, W. W., Jaeger, L., and other 5 authors:** Multifunctional RNA nanoparticles, Nano Lett., **14**, 5662–5671 (2014).
8. **Haque, F., Pi, F., Zhao, Z., Gu, S., Hu, H., Yu, H., and Guo, P.:** RNA versatility, flexibility, and thermostability for practice in RNA nanotechnology and biomedical applications, Wiley Interdiscip. Rev. RNA, **9**, e1452 (2018).
9. **Jasinski, D. L., Li, H., and Guo, P.:** The effect of size and shape of RNA nanoparticles on biodistribution, Mol. Ther., **26**, 784–792 (2018).
10. **Xu, Y., Pang, L., Wang, H., Xu, C., Shah, H., Guo, P., Shu, D., and Qian, S. Y.:** Specific delivery of delta-5-desaturase siRNA via RNA nanoparticles supplemented with dihomo-γ-linolenic acid for colon cancer suppression, Redox Biol., **21**, 101085 (2019).
11. **Wu, Q., Huang, L., and Zhang, Y.:** The structure and function of catalytic RNAs, Sci. China C Life Sci., **52**, 232–244 (2009).
12. **Lehnert, V., Jaeger, L., Michel, F., and Westhof, E.:** New loop-loop tertiary interactions in self-splicing introns of subgroup IC and ID: a complete 3D model of the *Tetrahymena thermophila* ribozyme, Chem. Biol., **3**, 993–1009 (1996).
13. **Guo, F., Gooding, A. R., and Cech, T. R.:** Structure of the Tetrahymena ribozyme: base triple sandwich and metal ion at the active site, Mol. Cell, **16**, 351–362 (2004).
14. **Woodson, S. A.:** Structure and assembly of group I introns, Curr. Opin. Struct. Biol., **15**, 324–330 (2005).
15. **Vicens, Q. and Cech, T. R.:** Atomic level architecture of group I introns revealed, Trends Biochem. Sci., **31**, 41–51 (2006).
16. **van der Horst, G., Christian, A., and Inoue, T.:** Reconstitution of a group I intron self-splicing reaction with an activator RNA, Proc. Natl. Acad. Sci. USA, **88**, 184–188 (1991).
17. **Doherty, E. A., Herschlag, D., and Doudna, J. A.:** Assembly of an exceptionally stable RNA tertiary interface in a group I ribozyme, Biochemistry, **38**, 2982–2990 (1999).
18. **Doudna, J. A. and Cech, T. R.:** Self-assembly of a group I intron active site from its component tertiary structural domains, RNA, **1**, 36–45 (1995).
19. **Ikawa, Y. and Inoue, T.:** Designed structural-rearrangement of an active group I ribozyme, J. Biochem., **133**, 189–195 (2003).
20. **Ikawa, Y., Shiraishi, H., and Inoue, T.:** *Trans*-activation of the *Tetrahymena* ribozyme by its P2-2.1 domains, J. Biochem., **123**, 528–533 (1998).
21. **Oi, H., Fujita, D., Suzuki, Y., Sugiyama, H., Endo, M., Matsumura, S., and Ikawa, Y.:** Programmable formation of catalytic RNA triangles and squares by assembling modular RNA enzymes, J. Biochem., **161**, 451–462 (2017).
22. **Rahman, M. M., Matsumura, S., and Ikawa, Y.:** Artificial RNA motifs expand the programmable assembly between RNA modules of a bimolecular ribozyme leading to application to RNA nanostructure design, Biology, **6**, E37 (2017).
23. **Ali, M. H. and Imperiali, B.:** Protein oligomerization: how and why, Bioorg. Med. Chem., **13**, 5013–5020 (2005).
24. **Royer, W. E., Jr., Zhu, H., Gorr, T. A., Flores, J. F., and Knapp, J. E.:** Allosteric hemoglobin assembly: diversity and similarity, J. Biol. Chem., **280**, 27477–27480 (2005).
25. **Aoto, S. and Yura, K.:** Case study on the evolution of hetero-oligomer interfaces based on the differences in paralogous proteins, Biophys. Physicobiol., **12**, 103–116 (2015).
26. **Williamson, C. L., Desai, N. M., and Burke, J. M.:** Compensatory mutations demonstrate that P8 and P6 are RNA secondary structure elements important for processing of a group I intron, Nucleic Acids Res., **17**, 675–689 (1989).
27. **Ikawa, Y., Moriyama, S., and Furuta, H.:** Facile syntheses of BODIPY derivatives for fluorescent labeling of the 3' and 5' ends of RNAs, Anal. Biochem., **378**, 166–170 (2008).
28. **Tanaka, T., Furuta, H., and Ikawa, Y.:** Installation of orthogonality to the interface that assembles two modular domains in the *Tetrahymena* group I ribozyme, J. Biosci. Bioeng., **117**, 407–412 (2014).
29. **Naito, Y., Shiraishi, H., and Inoue, T.:** P5abc of the Tetrahymena ribozyme consists of three functionally independent elements, RNA, **4**, 837–846 (1998).
30. **Gulshan, M. A., Rahman, M. M., Matsumura, S., Higuchi, T., Umezawa, N., and Ikawa, Y.:** Biogenic triamine and tetraamine activate core catalytic ability of *Tetrahymena* group I ribozyme in the absence of its large activator module, Biochem. Biophys. Res. Commun., **496**, 594–600 (2018).
31. **D'Ascenzo, L., Leonarski, F., Vicens, Q., and Auffinger, P.:** Revisiting GNRA and UNCG folds: U-turns versus Z-turns in RNA hairpin loops, RNA, **23**, 259–269 (2017).
32. **Herschlag, D. and Cech, T. R.:** Catalysis of RNA cleavage by the *Tetrahymena thermophila* ribozyme. 1. Kinetic description of the reaction of an RNA substrate complementary to the active site, Biochemistry, **29**, 10159–10171 (1990).
33. **Ishikawa, J., Furuta, H., and Ikawa, Y.:** An *in vitro*-selected RNA receptor for the GAAC loop: modular receptor for non-GNRA-type tetraloop, Nucleic Acids Res., **41**, 3748–3759 (2013).
34. **Jaeger, L. and Chworos, A.:** The architectonics of programmable RNA and DNA nanostructures, Curr. Opin. Struct. Biol., **16**, 531–543 (2006).
35. **Li, H., Lee, T., Dziubla, T., Pi, F., Guo, S., Xu, J., Li, C., Haque, F., Liang, X. J., and Guo, P.:** RNA as a stable polymer to build controllable and defined nanostructures for material and biomedical applications, Nano Today, **10**, 631–655 (2015).
36. **Geary, C., Chworos, A., Verzemnieks, E., Voss, N. R., and Jaeger, L.:** Composing RNA nanostructures from a syntax of RNA structural modules, Nano Lett., **17**, 7095–7101 (2017).
37. **Li, M., Zheng, M., Wu, S., Tian, C., Liu, D., Weizmann, Y., Jiang, W., Wang, G., and Mao, C.:** In *vivo* production of RNA nanostructures via programmed folding of single-stranded RNAs, Nat. Commun., **9**, 2196 (2018).
38. **Lee, C. H., Han, S. R., and Lee, S. W.:** Therapeutic applications of group I intron-based trans-splicing ribozymes, Wiley Interdiscip. Rev. RNA, **9**, e1466 (2018).
39. **Weng, D. E., Masci, P. A., Radka, S. F., Jackson, T. E., Weiss, P. A., Ganapathi, R., Elson, P. J., Capra, W. B., Parker, V. P., Lockridge, J. A., and other 3 authors:** A phase I clinical trial of a ribozyme-based angiogenesis inhibitor targeting vascular endothelial growth factor receptor-1 for patients with refractory solid tumors, Mol. Cancer Ther., **4**, 948–955 (2005).